OPTICAL IMAGING OF CELL MEMBRANE POTENTIAL CHANGES INDUCED BY APPLIED ELECTRIC FIELDS

DAVID GROSS,* LESLIE M. LOEW,‡ AND WATT W. WEBB*
*Applied and Engineering Physics, Cornell University, Ithaca, New York 14853; and ‡ Department of Chemistry, State University of New York, Binghamton, New York 13901

ABSTRACT We report the first imaging of the spatial distributions of transmembrane potential changes induced in nonexcitable cells by applied external electric fields. These changes are indicated by the fluorescence intensity of a charge-shift potentiometric dye incorporated in the cell plasma membrane and measured by digital intensified video microscopy.

Diverse biological responses to electric fields, both applied and endogenous, continue to motivate experimental searches for mechanisms of electromagnetic interactions with cells. It has been shown that development (1), regeneration (2–4), and repair (5) are all affected by electric fields and that many other basic cellular functions including motility (6–8) and receptor regulation (9) are modulated by applied external electric fields. In addition, cell membrane permeabilization and fusion have been effected by applied fields (10–12). Local perturbation of plasma membrane potentials provides a hypothetical mechanism of interaction of applied electric fields with cells. Exploratory measurements of the spatial distribution of perturbations of plasma membrane electric fields induced in cells by applied fields comprise the objective of the research reported in this article. The first digital video microscopy recordings of the fluorescence changes in an electric field-sensitive membrane soluble dye made these measurements possible. A preliminary description of these measurements has been reported at the Ionic Currents in Development Conference at the University of California, Los Angeles (13).

The use of optical detection methods for the measurement of fluorescence or absorption response to membrane electric fields in a dye-stained biological system was first reported in the early 1970s (14–17). Since that time, considerable advances in the design and production of field-sensitive optical dyes and concomitant advances in their application to biological problems have been reported (18–26). Of particular interest is the mapping of membrane electrical phenomena in different regions of a large cell or a group of cells (27–30). However, the spatial resolution of such measurements has been limited to the order of tens of micrometers by a need for fast detectors, usually photodiode arrays. For the study of the detailed spatial dependence of the membrane electric field in individual cells, digital video microscopy recording, and analysis provides the necessary higher resolution.

In this study we have employed a new styryl fluorescent indicator of membrane electric field, 1-(3-sulfonatopropyl)-4-[β] [2-(di-*n*-butylamino)-6-napthyl vinyl] pyridinium betaine (di-4-ANEPPS, number 27a in reference 26), developed by Loew and colleagues (26, 31). This probe was chosen for several reasons (32): (*a*) it responds linearly to membrane potential at the level of ~ 9% fluorescence change per 100 mV membrane potential change, (*b*) its absorption and emission spectral characteristics are well suited for microscopy, (*c*) it appears to incorporate reproducibly into one leaflet of an artifical bilayer, (*d*) the mechanism of its response to membrane potential is thought to be electrochromic in nature, and (*e*) the molecule has no net charge at neutral pH.

This chemical technology is combined with video microscopy measurements and digital image analysis that provide spatial and temporal quantitation of fluorescence light intensity images of individual cells. The fluorescence image of an epi-illuminated specimen formed in a Zeiss Universal research microscope (Carl Zeiss Inc., Thornwood, NJ) is detected by a Venus Scientific (Farmingdale, NY) three-stage intensifier video camera. The video signal is routed to a small video monitor as well as to the digitizing input of an image processing system (model GMR 274; Grinnell Systems, San Jose, CA). Live, stored and processed images are displayed on a high resolution color monitor (model C-3910; Mitsubishi Electric Co., Tokyo, Japan). Operation of the image processor and all associated peripherals including a 160 Mbyte hard disk (model 53160; Kennedy Co., Monrovia, CA) is under interactive computer control through a dedicated PDP 11/73 minicomputer. The di-4-ANEPPS fluorescence was

Dr. Loew's present address is Department of Physiology, University of Connecticut Health Center, Farmington, Connecticut 06032.

Please address correspondence to Watt W. Webb, Applied Physics, Clark Hall, Cornell University, Ithaca, New York 14853-2501.

excited by epi-illumination of the cells with a 546-nm peak of a mercury arc; the dichroic mirror had a 568-nm cutoff, and the barrier filter passed wavelengths above 590 nm. Digital processing of single or multiple images on a pixel-by-pixel basis is accomplished in the image processor to allow rapid spatial analysis of fluorescence light intensity. This technology allows us to examine the fluorescence response of cells at low dye dose and at low fluorescence excitation levels to avoid dye toxicity problems.

We studied several different cell types to assess the quantitative response of di-4-ANEPPS in single cells. Results are reported for four diverse cell types that are roughly spheroidal and thus simple to model, including: (*a*) A-431 cultured cells from a sustained line isolated from a human carcinoma, (*b*) rat basophilic leukemia (RBL) cells, (*c*) spores of the fungus *Uromyces appendiculatus* (Pers.) Ungar., and (*d*) protoplasts isolated from the root crown tissue of rye, *Secale cereale* L. cv Puma.

Membrane Potential Changes Induced in Single Cells by Applied Fields

Application of a uniform electric field E in conductive medium to cells of any size and of geometry that can be modeled as a uniform, ellipsoidal shell enclosing conductive cytoplasm should induce a calculable spatial alteration of membrane potential. When the membrane conductance can be neglected (33, 34) relative to the aqueous phases, the membrane potential change ΔV_m for a uniform spherical cell of radius a is given simply by a solution to Laplace's equation as

$$\Delta V_m = -(3/2)\,\mathrm{Ea}\cos\theta, \qquad (1)$$

where θ is the polar angle relative to the applied field. In this case the applied field is excluded from the cell interior that remains an equipotential while the external potential is enhanced by a factor of 3/2 at the cell surface by the resultant crowding of field lines. The membrane potential change is just the difference between the interior potential and the change of local exterior potential. The applied electric field can be considered effectively amplified within the cell membrane by 3/2 the ratio a/δ of cell radius to membrane thickness.

If the membrane conductivity is not negligible, the membrane potential changes given by Eq. 1 are, to first order, in the quasisteady state, reduced by the correction factor

$$2\sigma_o\sigma_i/[a(\sigma_m/\delta)(2\sigma_o + \sigma_i) + (2\sigma_o + \sigma_m)(2\sigma_m + \sigma_i)]. \qquad (2)$$

Here the conductivities of the exterior medium, intracellular medium, and membrane are respectively, σ_o, σ_i, and σ_m, and the effective membrane permeability is σ_m/δ. In typical nonexcitable cells in culture $\sigma_o \approx \sigma_i \approx 10^4\, a\sigma_m/\delta$ so the correction factor reduces to unity. Here we neglect all V_m dependence of the permeability.

For the case of an ellipsoidal cell of semimajor axes a_i, $i=1, 2, 3$, Eq. (1) generalizes (35–39) to the form

$$\Delta V_m = \sum_{i=1}^{3} K_i E_i x_i, \qquad (3)$$

where x_i are the three Cartesian coordinates of a point on the ellipsoid, E_i are the components of the applied field E, and $K_i = (1 + a_1a_2a_3A_i)^{-1}$. The constants A_i are elliptic integrals of the form

$$A_i = \int_0^\infty \mathrm{d}s/(s + a_i^2)\left[\sqrt{(s + a_1^2)(s + a_2^2)(s + a_3^2)}\right].$$

To prevent Joule heating by the extracellular currents, a special chamber (Fig. 1) for the application of large uniform fields to cells under the microscope was constructed. The coverslip on which the cells were growing was mounted with a small amount of silicon grease in a thin Plexiglas chamber such that the media bathing the cells was in contact with a pair of chlorided silver wire electrodes via media bridges in the interior of the Plexiglas chamber. The bathing medium, which was limited to 200μm thickness by coverslip spacers, also contacted the thin sapphire face of a second chamber that contained circulating cooling water. Sapphire was chosen for its high heat conductivity and optical transparence as it forms part of the microscope illumination pathway. The magnitude of the applied uniform field was calculated from the measured dimension of the chamber and the potential drop across it as measured by a pair of platinum wire electrodes connected to a voltmeter.

The applied field response of a large, distinctive, ellipsoidal A-431 cell is presented in Fig. 2 to illustrate the technique. This cell is unusual in its large size (24 × 15.4 μm), its isolation from more typical clusters of A-431 cells, and its distinctive marking by a bright contaminating particle at the upper left edge that saturates the camera and several smaller brightly fluorescent mobile contaminants around the cell periphery. These bright contaminants illustrate one difficulty in using dye fluorescence as a quantitative measure of membrane potential. The fluores-

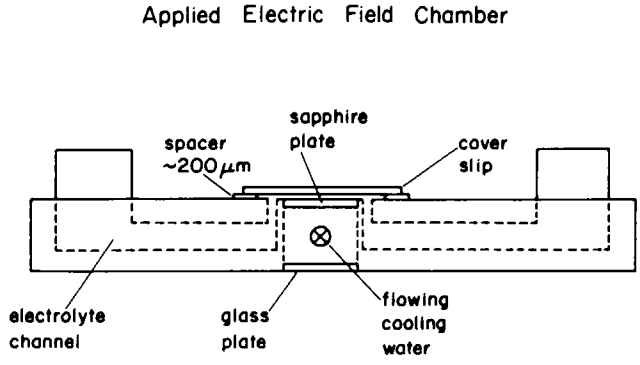

FIGURE 1 The Plexiglas microscope chamber for the application of uniform fields to cells. The flowing cooling water was necessary to prevent thermally-induced focus drift.

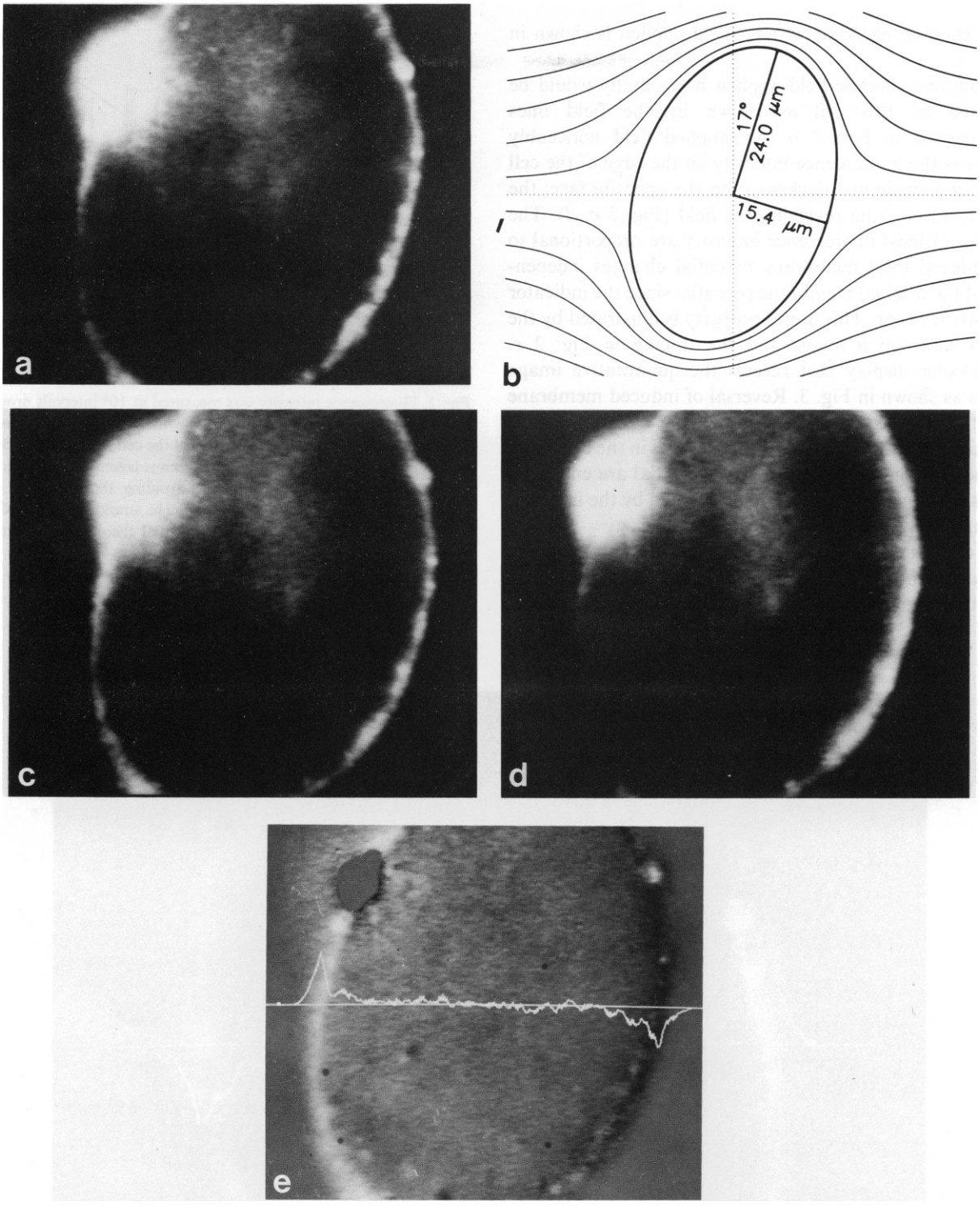

FIGURE 2 (*a*) A single A-431 human carcinoma cell stained for 10 min at 4 C with 10 μM di-4-ANEPPS in GIBCO Medium 199 + 10 mM HEPES, pH 7.3. The cell was grown in Dulbecco's Modified Eagle's Medium (DMEM) supplemented with 10% calf serum (both from GIBCO, Lawrence, MA). The bright contaminating marker at the upper left has saturated the camera. The microscope field of view excludes the transverse edges of this large cell. This image as well as all other raw images described here is a 30 video frame (1 s) average. (*b*) The measured cross-sectional dimensions of the cell closely fit that of an ellipse of major semiaxis 24 μm, minor semiaxis 15.4 μm and tilt of 17° from the vertical. Some field lines approximated from the solution of Laplace's law indicate the theoretical current flow around the cell. Since the cell membrane is assumably nonconducting, no electric current enters the cell. (*c*) The fluorescence response of the cell to an applied electric field of 53.0 V/cm directed from left to right. Note that in this figure the left part of the cell is hyperpolarized while the right is depolarized. (*d*) The fluorescence response to a 47.6 V/cm field directed from right to left. Note that the optical response is opposite to that of *c*. (*e*) The difference image produced by subtracting *d* from *c* on a pixel-by-pixel basis. Zero difference is mapped to a mid-grey level to display negative differences. The grey level scale has been expanded here for clarity. Because the oppositely directed fields in *c* and *d* produced opposite polarizations of the membrane between frames, the difference in *e* reflects only the potential-sensitive response of the dye. The value of the difference image intensity for a line of pixels across the center of the image is shown by the tracing. The width of the detected membrane-bound fluorescence intensity difference at either edge of the cell indicates the degree of spatial resolution attained. Each pixel in the center of this image represents a rectangular area in the object plane 0.09 × 0.08 μm^2, well below the optical resolution limit of the microscope. The width of the fluorescence difference peaks at cell edges is due mainly to the spreading of the contributions of fluorescence from nearly vertical curved membrane above and below the focal plane.

cence staining observed without field applied is shown in Fig. 2 *a*.

A uniform electric field applied horizontally would be distorted by this cell as shown by the field lines diagrammed in Fig. 2 *b*. An applied field noticeably brightens the fluorescence intensity on the edge of the cell facing the anode and darkens it on the opposite face; the polarity reverses on reversing the field (Fig. 2 *c*, *d*). The changes of local fluorescence intensity are proportional to the induced local membrane potential changes independent of the original membrane potential since the indicator response is linear. This useful property is illustrated by the digital subtraction image and the tracing in Fig. 2 *e*. Pseudocolor display best reveals the quantitative image details as shown in Fig. 3. Reversal of induced membrane potential changes produced by switching the applied field direction reverses the fluorescence changes in the cell. Only the induced changes of membrane potential are enhanced in this difference image as is demonstrated by the intensity tracing in Fig. 2 *e*.

A quantitative estimate of response is obtained by comparing measurements of relative fluorescence change, with the theoretical induced membrane potential charge given by Eq. 3. Thus, the fluorescence intensity of the cell

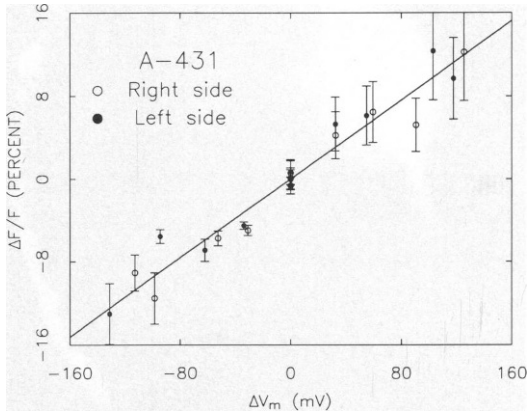

FIGURE 4 The quantitative response of di-4-ANEPPS in the cell of Fig. 2. Fluorescence intensity was measured at 10° intervals around the cell perimeter and compared with the induced membrane potential calculated from Eq. 3 for the geometry of the cell shown above. Both the optical response and the calculated membrane potential distribution were averaged over each side of the cell, avoiding the region of camera saturation at the *upper left* of panel 2 a. The straight line fit to the data has slope 9.5%/ 100 mV membrane potential change with a correlation coefficient $r = 0.974$.

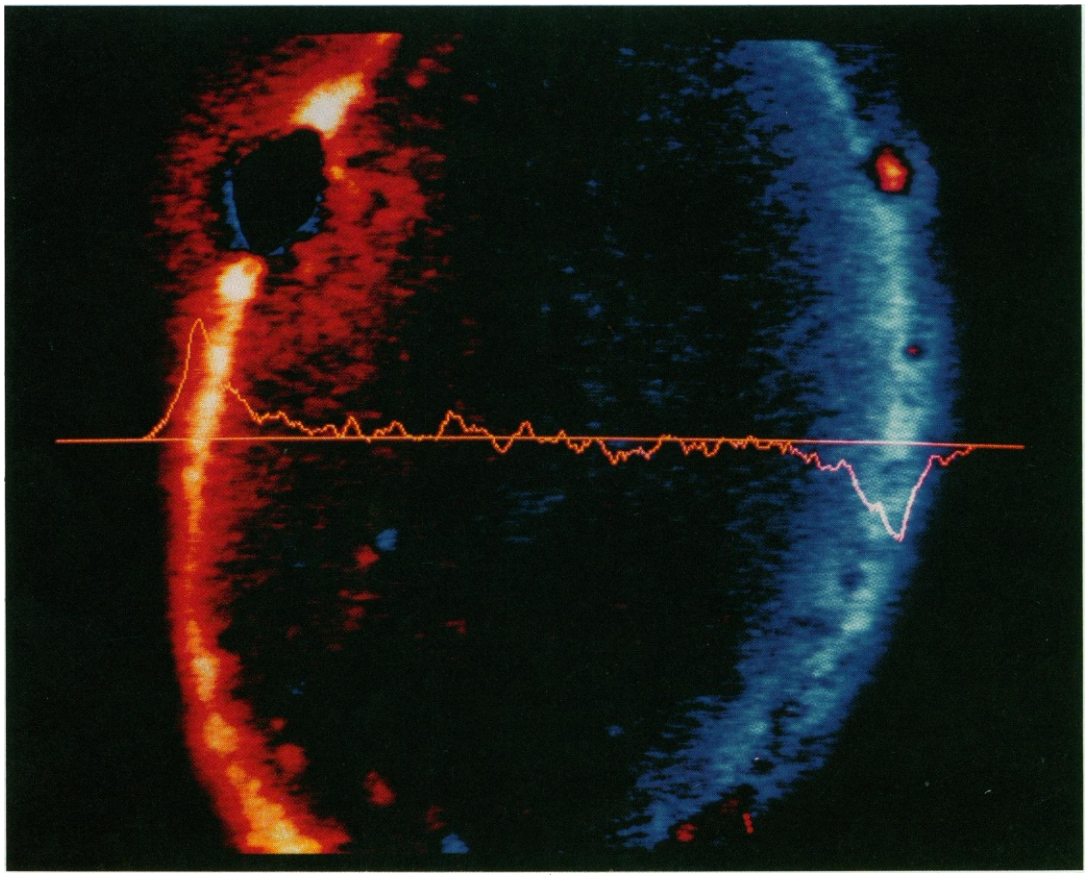

FIGURE 3 Pseudocolor display of the difference image of Fig. 2*e*. Red indicates positive fluorescence change, blue negative. The color intensity scales with fluorescence intensity difference.

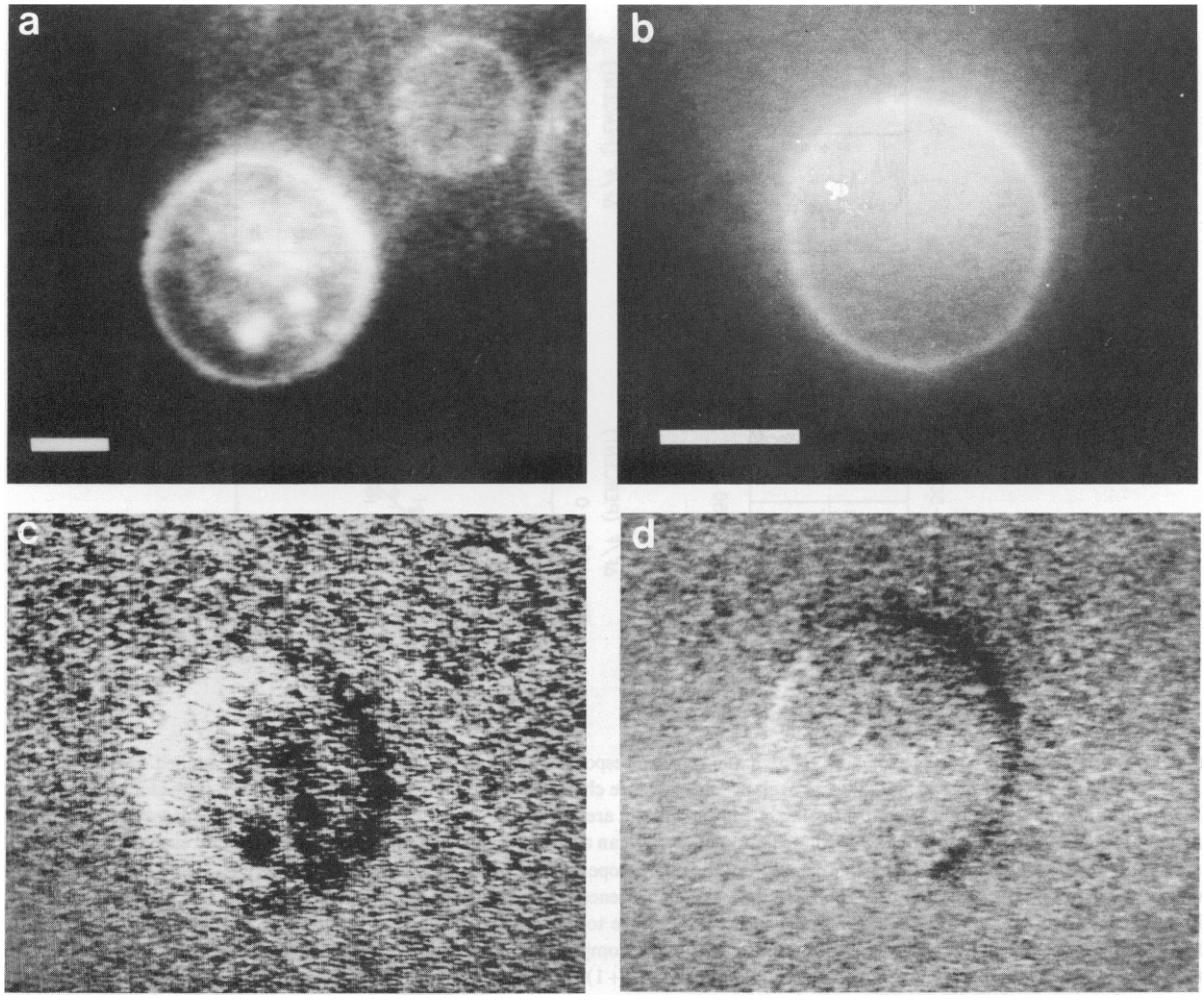

FIGURE 5 (*a*) The fluorescence image of a single RBL cell that was stained with 3 μM di-4-ANEPPS in Tyrode's solution for 10 min at 4°C. The cells were plated onto coverslips from a cell suspension for 10 min at 37°C immediately before staining. The cells were grown in Eagle's minimum essential medium plus 20% fetal calf serum (GIBCO). Bar = 10 μm. (*b*) The fluorescence image of a *S. cereale* protoplast stained with 10 μM di-4-ANEPPS in a sorbitol solution of 0.530 OsM. The protoplasts were pipetted onto a coverslip coated with concanavalin A for 5 min; they were then stained for 10 min at 4°C. Bar = 10 μm. (*c*) The response of the RBL-cell-associated fluorescence for an applied field of 31 V/cm directed to the right minus that for a 31 V/cm field directed to the left. The grey scale has been expanded to improve image contrast. (*d*) Same as for *c* except for the protoplast with field strengths of $\pm$59 V/cm.

in Fig. 2 was measured along the periphery in the field of view at 10° angular intervals for each of 11 images of the cell exposed to electric fields of various magnitudes and of both directions. These data were normalized for angular position, corrected for photobleaching and averaged over the left and right sides of the cell, avoiding the bright inclusion at the upper left. The results plotted in Fig. 4 show that the induced fluorescence changes in both sides of the cell respond identically at the level of 9.52 $\pm$ 0.02% fluorescence change per 100 mV of induced membrane potential, a response that is consistent with the value of 9% obtained for this dye in artificial membranes (32).

We observed the expected angular dependence of Eq. 1 in several types of small quasi-spherical RBL cells, *S. cereale* protoplasts, and *U. appendiculatus* spores. Two nearly spherical cells that we examined are shown in Fig. 5. The fluorescence image of each cell at zero applied field, an RBL on the left and a rye protoplast on the right, is shown in the *top panels*. The *bottom panels* show the fluorescence difference in response to fields of $\pm$31 and $\pm$59 V/cm, respectively. Both difference images are right-directed field image minus left-directed field image.

The spatial distribution and magnitudes of the fluorescence changes in response to applied fields in the two small cells of Fig. 5 were measured under interactive semi-automated computer control. Some typical angular distributions of relative fluorescence change at different applied field strengths are shown in Fig. 6 *a* for the cells of Fig. 5. A nonlinear least-squares fit to the function $\Delta F/F = A + B\cos\theta$ was performed for all images collected for each cell; the results are shown in Fig. 6 *b*, *c*. The results from these cells as well as from the A-431 cell of Fig. 2 and a *U.*

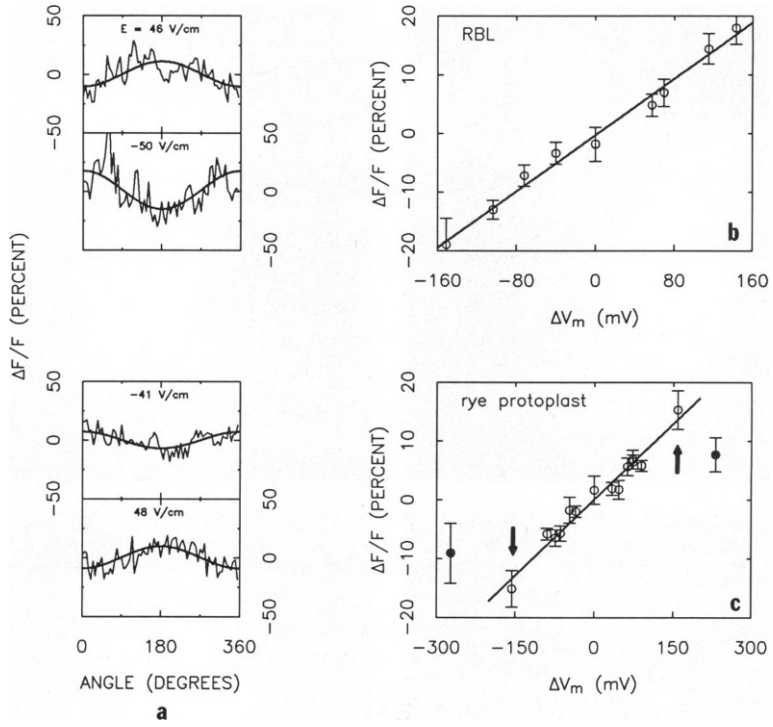

FIGURE 6 (*a*) The angular dependence of relative fluorescence response of the two cells of Fig. 2 at different applied field strengths and directions. The data, shown by the light lines, are relative fluorescence changes calculated from intensities collected from stored digital images at five-degree angular resolution around the cell while the solid lines are the result of the computer nonlinear least-squares fit to the equation $\Delta F/F = A + B\cos\theta$. At each five-degree increment around the cell, an area of 5 × 5 pixels was averaged to generate each data point. At this magnification, 5 pixels is the expected resolution limit of the microscope optics. The two *top* panels are for the RBL cell while the two *bottom* panels are for the *S. cereale* protoplast. The RBL data are fluorescence change for field-applied images relative to a single field-off image, while the protoplast data are for single field-applied images relative to the average of all 5 field-off images. (*b*) Response of the RBL cell fluorescence to induced membrane potential as obtained from the computer fit. The vertical axis is the coefficient B of the fit corrected for changing levels of total membrane fluorescence by the factor $1/(A+1)$. The straight line is the least-squares fit to the data; it represents a fluorescence response of 12.0% per 100 mV of membrane potential with a correlation coefficient of $r = 0.99$. (*c*) As in *b* except for the protoplast. The response is 8.6% per 100 mV with a correlation of $r = 0.98$. After application of the fields of +97 V/cm and −100 V/cm (arrows), the total cell fluorescence increased and large internal vesicles were formed, stained with dye. Further increases in applied fields showed decreased response (solid circles) indicating that the protoplast had been permeabilized by the high fields and/or excess nonresponding dye had entered or crossed the cell membrane.

TABLE I
RESPONSE OF DI-4-ANEPPS FLUORESCENCE IN SINGLE CELLS RESPONDING TO EXTERNALLY APPLIED ELECTRIC FIELDS

Cell type	Dye response
	%/100 mv
A-431	9.52 ± 0.02
rye protoplast	8.6 ± 1.4
fungus spore*	3.7 ± 2.0
RBL‡	12.0 ± 1.5

*This somewhat irregularly shaped spore was aspirated onto a cover slip in 1 mM TRIS buffer, stained with 1 μM di-4-ANEPPS in the buffer, and mounted in the chamber as for the other cells.

‡The zero-field fluorescence fluctuated substantially on two other RBL cells during measurements made on different days with different batches of cells. Their measured dye responses were 7.8 and 9.5 with large uncertainties. These tumor basophils are known to depolarize upon antigen stimulation (46–48); thus a shifting "zero" might be indicative of external field induced electric activity.

appendiculatus spore also examined are summarized in Table I.

Exploratory Observations of Cell-Cell Interactions

The response of clusters of A-431 cells stained with di-4-ANEPPS to an applied electric field was examined to explore the applicability of this technique to cellular systems more complicated than isolated single cells. In the *left panels* of Fig. 7 are the zero-field fluorescence images of several clumps of A-431 cells. Why the regions of contact between these A-431 cells are more than twice as bright as the peripheral membranes is not understood, but may reflect a larger membrane area due to unresolved membrane folds, summated contributions of fluorescence along a vertical membrane segment, or heavier staining in the contact area. The responses of these cells to applied

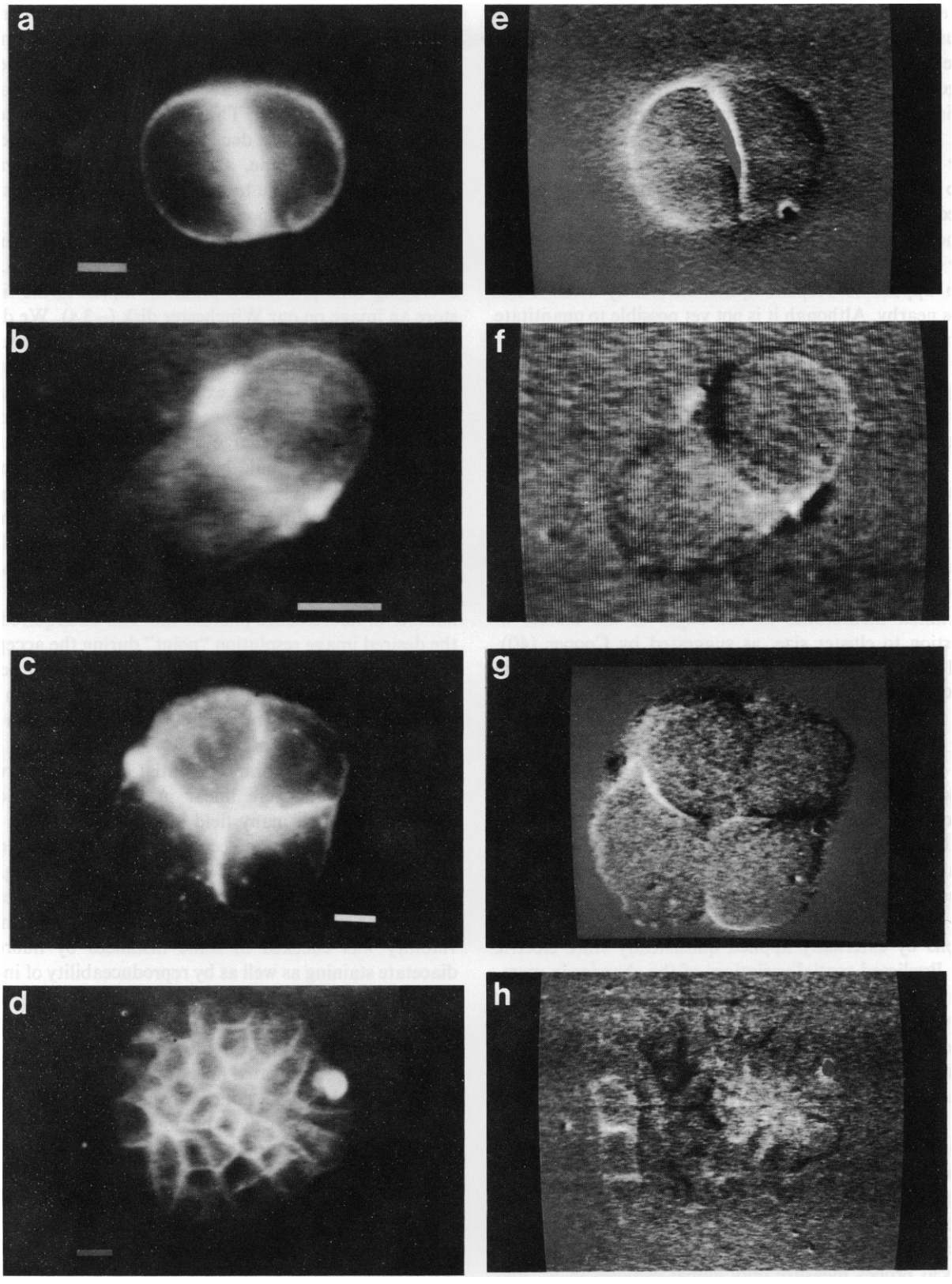

FIGURE 7 (*a–d*) The fluorescence images of groups of A-431 cells stained with 3 μM di-4-ANEPPS. The original data image for panel *b* was digitally zoomed by a factor of 2. Bars are 10 μm in panels *a* and *c*, and 20 μm in panels *b* and *d*. (*e–h*) Difference images as in Figs. 1 *e* and 2 *c*, *d*. Field strengths and directions were 42 V/cm field right minus no field image *e*, 40 V/cm field left minus 42 V/cm field right *f*, 24 V/cm field right minus no field image *g*, and 31 V/cm field right minus 46 V/cm field left *h*.

fields are shown in the *right panels* of Fig. 7, which show various applied field difference images like Figs. 3 and 5.

The distribution of induced membrane potential changes for groups of two cells is qualitatively similar to the distribution expected for two hemispherical cells of equal diameter joined at their flat faces. However, for larger clumps, the measured response is not intuitive. The clump of four cells (Fig. 7 *c*, *g*) responds strongly to the applied field in some areas where one would naively assume little induced membrane potential change. In the larger clump, Fig. 7 *d*, *h*, groups of several cells within the clump appear to respond quite differently from other groups nearby. Although it is not yet possible to quantitate the observation in such clumps of cells, it appears qualitatively that some groups of cells within these multicellular aggregates were collectively hyperpolarized by the applied field while others appeared depolarized. At the periphery of these clumps the magnitudes of the maximum fluorescence change and thus the induced ΔV_m values for a given applied field strength are qualitatively independent of clump size and are of the same magnitude as those in isolated single cells. Thus, intercellular electrical connections are apparently not strong enough to form an effective electrical continuum that would increase the induced ΔV_m at terminal membranes at the edges of the cluster in proportion to cluster size, as suggested by Cooper (40). A-431 cells are not known to form intercellular electrical connections such as gap junctions.

DISCUSSION

We have demonstrated that a membrane-bound fluorescent optical probe of membrane potential can provide digital video images of stained cells for measurements of spatial distributions of membrane potential changes with the resolution of the optical microscope. We have investigated membrane potential changes induced in nonexcitable cells by externally applied quasisteady state electric fields. Predicted spatial variations of the changes in membrane potential induced in some cells of simple shape are confirmed for the first time. We have found that the induced membrane potential changes in spherical cells vary about the cell as the cosine of the angle from the applied field direction as predicted by elementary theory. This effect has been implied by other measurements (41–43) but has not previously been shown directly.

Note that measurements of the spatial distribution of membrane potential even in cells of simple geometry are not possible with nonlocal probes such as microelectrodes or charged redistribution dyes or radioisotopic tracers. Nonlocal probes measure only global changes in V_m and not spatial variations such as that of Eq. 1, which average to zero over the whole cell. Thus only local membrane potential probes such as the membrane soluble dye di-4-ANEPPS can monitor such spatial distributions of V_m.

Fluorescence imaging for V_m measurements represents a compromise between spatial and temporal resolution. The intrinsic local measurement accuracy of such imaging techniques is ultimately limited by the signal-to-noise ratio (S/N) of the detected fluorescence in the regions of interest of the image. The S/N can be increased by increasing fluorophore density, excitation light intensity, image integration time, and scale of spatial averaging, each improvement due to the decreased statistical significance of all noise components, including shot noise.

As noted above, all of our cell images were obtained by averaging 1 s, i.e., 30 frames, of the video signal. This averaging time provided a practical match to the time to store an image on our Winchester disk (~3 s). We did not explore explicitly the dependence of S/N and thus the accuracy of the measurement of ΔV_m on integration time.

Our impression is that extrinsic perturbations such as light scattering, fluorescence of nonresponding dye, and cell motion were the source of the limiting uncertainties. All of these effects could be further reduced if necessary. The gain in spatial resolution of the imaging technique we describe is offset by loss of temporal resolution. There is always a trade-off between temporal and spatial resolution. However, when necessary, both can be optimized beyond what we found sufficient. The controlling parameter is the number of fluorescence photons that can be acquired from the desired image resolution "point" during the acceptable recording time. The measurement hardware can be optimized for fast recording with low spatial resolution using diode array detectors or for high spatial resolution using video or CCD detectors.

The induced membrane potential changes observed in several cell types were linear in the applied field and reversible through many field applications of both signs. Irreversible cell damage occurred with large applied field strengths in the presence of dye as illustrated in Fig. 6 for rye protoplasts; freshly trypsinized A-431 cells were damaged in the presence of dye by fields of $\simeq$50 V/cm. Cell viability was checked in some instances by fluorescein diacetate staining as well as by reproduceability of induced membrane potential changes. We noted that a convenient assay of cell viability was the exclusion of di-4-ANEPPS fluorescence from the cell interior; injured cells rapidly took up the dye. Repeated field applications below damage threshold levels did not noticeably increase cell death.

The generation of calculable membrane potential shifts by application of external electric fields in single, simple, nonexcitable cells provides a useful tool for the calibration of the response of optical membrane potential probes. Since the method provides controllable relative changes in membrane potential, independent of the absolute resting potential, calibration reference is easy to establish, at least for cells behaving simply. Such a reference level has been difficult to obtain by other methods.

However, as formula (2) shows, the conductance σ_m of the plasma membrane can reduce the response of cell membrane potential to an applied electric field. Only if the

membrane permeability σ_m/δ is much smaller than the ratios to the cell size of the cytoplasmic and medium conductivities, σ_i/a and σ_o/a, does the induced membrane potential change become independent of membrane permeability. This effect has been demonstrated (results not shown) by permeabilizing freshly plated A-431 cells with $\simeq$50 V/cm field pulses which cause the formation of large plasma membrane blebs. These blebbed cells show no fluorescence change with applied field as expected if they are highly permeable. Note that the expected absence of resting membrane potential in this case is not readily detected with optical probes since an absolute reference level is difficult to obtain.

This effect of membrane permeability may account for some of the cell to cell differences in dye response of RBL cells and the low response of the spore noted in Table I. The spore was bathed in relatively low conductivity medium, which enhances the shunting effect of membrane permeability. The membrane electric field sensitivity of the dye may vary among the membranes of different types of cells due to the intervention of nonelectrochromic mechanisms (44). In fact, some electrochromic dyes appear to show enhanced response of unknown origin in some cell preparations (29). However, the dye may not remain confined to the membrane bilayer outer leaflet in all cell types leading to diminished sensitivity. Indeed, internal membrane staining appears in many cell types after times of the order of an hour; among these cells are the sustained lines of normal rat kidney (NRK), GM3348 human fibroblasts, L5 myoblasts, and the germ tubes of germinating *U. appendiculatus* spores. Preliminary results with other "charge-shift" probes containing longer hydrocarbon sidechains or net electric charges suggest that these staining problems can be solved in many more cell types. Thus the characteristic calibration factor of 9%/100 mV for di-4-ANEPPS should be used with caution, and preferably determined for each cell type and condition. Our staining protocol (see legends to Figs. 2 and 5) was intended to maximize the incorporation of dye into the plasma membrane while minimizing dye internalization. The membrane staining was nearly independent of dye concentration in the staining medium between 3 and 10 μM.

It is necessary to consider whether tangential electric fields induce enough dye electrophoresis in cell plasma membranes (34, 45) to contribute to the fluorescence intensity changes in response to an applied field. This process can be excluded in the present studies by two observations. First, the rate of dye migration over the tens of microns of path length on individual cells and across cell boundaries in the clumps is not sufficient to affect its distribution during our measurement times of $\simeq$2 s. If incipient segregation were appreciable, it should also have appeared as a slow intensity transient after reversing fields, but it did not. Second, a direct test was provided by the application of $\simeq$50 V/cm fields (data not shown) to produce leakiness and blebs in freshly-plated A-431 cells. As expected, all detectable fluorescence response to applied fields was lost on these leaky cells and their blebs during subsequent lower field applications. However, electrophoresis should be nearly as effective on blebbed cells, since it depends on the tangential component of the applied electric field; thus electrophoresis is again excluded. Therefore, we conclude that only the potentiometric response of the dye contributes to the signals we have measured. Electrophoretic migration of membrane-soluble potential sensing dyes might perturb much longer duration experiments.

We found that cell clumps of complicated geometry also respond to an applied external field with spatially-varying membrane potential changes. However, the distribution of induced membrane potential changes is considerably more complex than for single cells, and is not yet quantitatively interpretable. Groups of cells within a clump in culture do appear qualitatively to be capable of local cooperative response to applied electric fields, since the membrane potential changes in some regions of the clump are only hyperpolarizing or depolarizing, i.e., the characteristic symmetric spatial response of ΔV_m occurs over clump dimensions rather than cell dimensions. The controlling features of this response remain to be determined by application of the spatially-resolved optical fluorescent probe methods for membrane potential measurement. Analysis of groups of cultured cells in monolayers appears promising, but tissue may be intractable. The complex behavior observed in single layer clusters implies even less intuitive electric field responses of tissue that have yet to be studied. However, the fact that the behavior of single cells can be nicely understood in terms of a simple linear model provides encouragement that the more complex systems will also be amenable to analysis.

We wish to thank Clare Fewtrell and David Holowka for supplying RBL cells, Thomas Björkman and Peter Steponkus for supplying the rye seedling protoplasts, Richard Staples for supplying the *U. appendiculatus* spores, and Christine Coulter for her tissue culture assistance.

This work was supported by grants from the Office of Naval Research (N00014-84-K-0390), the National Science Foundation (PCM-83-03404), the Cornell Biotechnology Program (David Gross and Watt W. Webb) and by the National Institutes of Health (GM25190 and GM35063) and a Research Career Development Award (CA00677) from the National Cancer Institute (Leslie M. Loew).

Received for publication 9 September 1985 and in final form 13 February 1986.

REFERENCES

1. Jaffe, L. F. 1979. Control of development by ionic currents. *In* Membrane Transduction Mechanisms. R. A. Cone and J. E. Downing, editors. Raven, New York. 199–231.
2. Borgens, R. B., J. W. Vanable, Jr., and L. F. Jaffe. 1977. Bioelectricity and regeneration. I. Initiation of frog limb regeneration by minute currents. *J. Exp. Zool.* 200:403–416.
3. Borgens, R. B., E. Roederer, and M. J. Cohen. 1981. Enhanced spinal cord regeneration in lamprey by applied electric fields. *Science (Wash. DC).* 213:611–617.

4. Jaffe, L. F., and M-m. Poo. 1979. Neurites grow faster towards the cathode than the anode in a steady field. *J. Exp. Zool.* 209:115–128.
5. Kenner, G. H., E. W. Gabrielson, J. E. Lovell, H. E. Marshall, and W. S. Williams. 1975. Electrical modification of disuse osteoporosis. *Calcif. Tissue Res.* 18:111–117.
6. Luther, P. W., H. B. Peng, and J. J-C. Lin. 1983. Changes in cell shape and actin distribution induced by constant electric fields. *Nature (Lond.).* 303:61–64.
7. Cooper, M. S., and R. E. Keller. 1984. Perpendicular orientation and directional migration of amphibian neural crest cells in dc electrical fields. *Proc. Natl. Acad. Sci. USA.* 81:160–164.
8. Cooper, M. S., and M. Schliwa. 1985. Electrical and ionic controls of tissue cell locomotion in dc electric fields. *J. Neurosci. Res.* 13:223–244.
9. Young, S. H., and M-m. Poo. 1983. Topographical rearrangement of acetylcholine receptors alters channel kinetics. *Nature (Lond.).* 304:161–163.
10. Zimmermann, U., and J. Vienken. 1982. Electric field-induced cell-to-cell fusion. *J. Membr. Biol.* 67:165–182.
11. Tessie, J., V. P. Knutson, T. Y. Tsong, and M. D. Lane. 1982. Electric pulse-induced fusion of 3T3 cells in monolayer culture. *Science (Wash. DC).* 216:537–538.
12. Knight, D., and P. F. Baker. 1982. The chromaffin granule proton pump and calcium-dependent exocytosis in bovine adrenal medullary cells. *J. Membr. Biol.* 68:107–140.
13. Gross, D., L. M. Loew, T. A. Ryan, and W. W. Webb. 1985. Spatially-resolved optical imaging of membrane potentials induced by applied electric fields. In Ionic Currents in Development. R. Nuccitelli, editor. Alan R. Liss, Inc., New York. 263–270.
14. Davila, H. V., B. M. Salzberg, L. B. Cohen, and A. S. Waggoner. 1973. A large change in axon fluorescence that provides a promising method for measuring membrane potential. *Nature New Biol.* 241:159–160.
15. Salzberg, B. M., H. V. Davila, and L. B. Cohen. 1973. Optical recording of impulses in individual neurones of an invertebrate central nervous system. *Nature (Lond.).* 246:508–509.
16. Cohen, L. B., B. M. Salzberg, H. V. Davilla, W. N. Ross, D. Landowne, A. S. Waggoner, and C. H. Wang. 1974. Changes in axon fluorescence during activity: molecular probes of membrane potential. *J. Membr. Biol.* 19:1–36.
17. Tasaki, I. 1974. Energy transduction in the nerve membrane and studies of excitation processes with extrinsic fluorescence probes. *Ann. NY Acad. Sci.* 227:247–276.
18. Cohen, L. B., and B. M. Salzberg. 1978. Optical measurements of membrane potential. *Rev. Physiol. Biochem. Pharmacol.* 83:35–88.
19. Loew, L. M., S. Scully, L. Simpson, and A. S. Waggoner. 1979. Evidence for a charge-shift electrochromic mechanism in a probe of membrane potential. *Nature (Lond.).* 281:479–499.
20. Waggoner, A. S. 1979. Dye indicators of membrane potential. *Annu. Rev. Biophys. Bioeng.* 8:47–68.
21. Gupta, R. K., B. M. Salzberg, A. Grinvald, L. B. Cohen, K. Kamino, S. Lesher, M. B. Boyle, A. S. Waggoner, and C. H. Wang. 1981. Improvements in optical methods for measuring rapid changes in membrane potential. *J. Membr. Biol.* 58:123–137.
22. Grinvald, A., R. Hildesheim, I. C. Farber and L. Anglister. 1982. Improved fluorescent probes for the measurement of rapid changes in membrane potential. *Biophys. J.* 39:301–308.
23. Salzberg, B. M., A. L. Obaid, D. M. Senseman, and H. Gainer. 1983. Optical recording of action potentials from vertebrate nerve terminals using potentiometric probes provides evidence for sodium and calcium components. *Nature (Lond.).* 306:36–40.
24. Grinvald, A., L. Anglister, J. A. Freeman, R. Hildesheim, and A. Manker. 1984. Real-time optical imaging of naturally evoked electrical activity in intact frog brain. *Nature (Lond.).* 308:848–850.
25. Loew, L. M., G. W. Bonneville, and J. Surow. 1978. Charge shift probes of membrane potential. Theory. *Biochemistry.* 17:4065–4071.
26. Hassner, A., D. Birnbaum, and L. M. Loew. 1984. Charge shift probes of membrane potential. Synthesis. *J. Org. Chem.* 49:2546–2551.
27. Ross, W. N., and V. Krauthamer. 1984. Optical measurements of potential changes in axons and processes of neurons of a barnacle ganglion. *J. Neurosci.* 4:659–672.
28. Krauthamer, V., and W. N. Ross. 1984. Regional variations in excitability of barnacle neurons. *J. Neurosci.* 4:673–682.
29. Grinvald, A., A. Fine, I. C. Barber, and R. Hildesheim. 1983. Fluorescence monitoring of electrical responses from small neurons and their processes. *Biophys. J.* 42:195–198.
30. Grinvald, A. 1984. Real-time optical imaging of neuronal activity. *Trends Neurosci.* 7:143–150.
31. Loew, L. M. 1982. Design and characterization of electrochromic membrane probes. *J. Biochem. Biophys. Methods* 6:243–260.
32. Fluhler, E., V. G. Burnham and L. M. Loew. 1985. Spectra, membrane binding and potentiometric responses of new charge shift probes. *Biochemistry.* 24:5749–5755.
33. Jaffe, L. F., and R. Nuccitelli. 1977. Electrical controls of development. *Annu. Rev. Biophys. Bioeng.* 6:445–476.
34. Poo, M.-m. 1981. In situ electrophoresis of membrane components. *Annu. Rev. Biophys. Bioeng.* 10:245–276.
35. Maxwell, J. C. 1892. A Treatise on Electricity and Magnetism, Vol. 1. Oxford University Press, London. 237–240.
36. Stratton, J. A. 1941. Electromagnetic Theory. McGraw-Hill, Inc., New York. 207–217.
37. Fricke, H. 1924. A mathematical treatment of the electric conductivity and capacity of disperse systems. I. The electric conductivity of a suspension of homogeneous spheroids. *Phys. Rev.* 24:575–587.
38. Cole, K. S. 1968. Membranes, Ions and Impulses. University of California Press, Berkeley. 12–38.
39. Bernhardt, J., and H. Pauly. 1973. On the generation of potential differences across the membranes of ellipsoidal cells in an alternating electric field. *Biophysik.* 10:89–98.
40. Cooper, M. S. 1984. Gap junctions increase the sensitivity of tissue cells to exogenous electric fields. *J. Theor. Biol.* 111:123–130.
41. Farkas, D. L., R. Korenstein, and S. Malkin. 1980. Electroselection in the photosynthetic membrane: polarized luminescence induced by an external electric field. *FEBS (Fed. Eur. Biochem. Soc.) Lett.* 120:236–242.
42. Farkas, D. L., R. Korenstein, and S. Malkin. 1984. Electrophotoluminescence and the electrical properties of the photosynthetic membrane. I. Initial kinetics and the charging capacitance of the membrane. *Biophys. J.* 45:363–373.
43. Knight, D. E. 1981. Rendering cells permeable by exposure to electric fields. *Tech. Cell Physiol.* P113:1–20.
44. Loew, L. M., L. B. Cohen, B. M. Salzberg, A. L. Obaid, and F. Bezanilla. 1985. Charge shift probes of membrane potential: characterization of aminostyrylpyridinium dyes on the squid giant axon. *Biophys. J.* 47:71–77.
45. McLaughlin, S., and M.-m. Poo. 1981. The role of electro-osmosis in the electric-field-induced movement of charged macromolecules on the surfaces of cells. *Biophys. J.* 34:85–93.
46. Sagi-Eisenberg, R., and I. Pecht. 1983. Membrane potential changes during IgE-mediated histamine release from rat basophilic leukemia cells. *J. Membr. Biol.* 75:97–104.
47. Kanner, B. I., and H. Metzger. 1983. Crosslinking of the receptors for immunoglobulin E depolarizes the plasma membrane of rat basophilic leukemia cells. *Proc. Natl. Acad. Sci. USA.* 80:5744–5748.
48. Kanner, B. I., and H. Metzger. 1984. Initial characterization of the calcium channel activated by the cross-linking of the receptors for immunoglobulin E. *J. Biol. Chem.* 259:10188–10193.